COMBINED BUOYANCY- AND PRESSURE-DRIVEN FLOW THROUGH A SHALLOW, HORIZONTAL, CIRCULAR VENT

Leonard Y. Cooper
Building and Fire Research Laboratory
National Institute of Standards and Technology
Gaithersburg, Maryland

ABSTRACT

Combined buoyancy- and pressure-driven (i.e., forced) flow through a horizontal vent is considered where the vent-connected spaces are filled with fluids of different density in an unstable configuration (density of the top is larger than that of the bottom). With zero-to-moderate cross-vent pressure difference, Δp, the instability leads to bi-directional exchange flow between the two spaces. For relatively large Δp, the flow through the vent is uni-directional, from the high- to the low-pressure space. An anomaly of a standard vent flow model, which uses Bernoulli's equation with a constant flow coefficient, C_D, is discussed. Thus, the standard model does not predict expected bi-directional flows at small-to-moderate Δp or non-zero flow at $\Delta p = 0$. Also, when Δp exceeds the critical value, Δp_{FL}, which defines the onset of uni-directional or "flooding" flow, there is a significant dependence of C_D on the relative buoyancy of the upper and lower fluids (i.e., C_D is not constant). Finally, the location of the high-pressure side of the vent, i.e., top or bottom, can be expected to influence vent flow characteristics.

Analysis of the relevant boundary value problems and of available experimental data lead to a general mathematical model of the vent flow which removes the anomaly of the standard model and which takes all the above effects into account. The result is an algorithm to calculate flow through shallow, horizontal, circular vents under high-Grashof number conditions.

INTRODUCTION

Consider the flow through a horizontal vent where the fluids in the vent-connected spaces near the elevation of the vent are of arbitrary density. Assume that in each space, away from the vent, the environment is relatively quiescent with pressure well approximated by the hydrostatic pressure. As in Figure 1, designate the spaces as TOP and BOTTOM and let subscripts

T and B refer to conditions in these respective spaces near the vent elevation, but removed far enough laterally so that variations to the quiescent far-field environment, due to vent flows that may exist, are negligible. $\dot{V}_T$ and $\dot{V}_B$ are the volume flow rates through the vent from top to the bottom side of the vent and from the bottom to the top side of the vent, respectively. Flow through the vent is determined by: the design of the vent, its shape and its depth, L; the densities, ρ_T and ρ_B; and the cross-vent pressure difference

$$\Delta p = p_H - p_L \geq 0; \quad p_H = \max(p_T, p_B); \quad p_L = \min(p_T, p_B) \quad (1)$$

Subscripts H and L will always refer to the conditions on the HIGH- and LOW-pressure sides of the vent, respectively. When $\Delta p = 0$, the high-/low-pressure designations are arbitrary. In cases where gas flows are involved, Δp is assumed to be small compared to p_B and p_T.

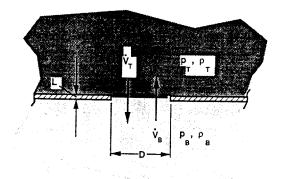$$\Delta p / \bar{p} << 1; \quad \bar{p} = (p_H + p_L)/2 = (p_B + p_T)/2 \quad (2)$$

FIGURE 1. THE HORIZONTAL VENT CONFIGURATION.

The objective of this work is to develop a mathematical model for predicting, for arbitrary specified p_T and p_B, the rates of flow though the vent under conditions involving unstable configurations, where a relatively dense fluid in the upper space overlays a less dense fluid in the lower space.

$$\Delta \rho = \rho_T - \rho_B > 0 \qquad (3)$$

With zero-to-moderate $\Delta \rho$, the instability leads to bi-directional exchange flow between the two spaces. As the flows enter the upper and lower spaces they are upward- and downward-buoyant, respectively, and they rise and fall as plumes to the far field. For relatively large $\Delta \rho$, the vent flow is uni-directional, from high to low pressure. Sufficiently deep into the low-pressure space, the flow is dominated by buoyancy forces and it continues to the far field as a buoyant plume.

Only quasi-steady features of the flows being studied will be discussed and analyzed. Thus, even when the flows are fluctuating it is assumed that time scales which characterize their fluctuations are relatively small i.e., meaningful average flow characteristics can be established, in principle, with integrals over time intervals which are relatively small compared to characteristic times of interest.

The Standard Vent Flow Model and Its Shortcomings

There exists a simple, effective model for estimating the flow through both horizontal and vertical vents which is nearly always used in practical applications, e.g., in the modeling of compartment fire phenomena. The model, referred to here as the *standard* model, uses Bernoulli's equation and an orifice flow coefficient, C_D, to compute the rate of flow through the vent. For horizontal vents, Δp and velocity are estimated to be uniform across the vent.

There is a basic problem with the standard model in the case of horizontal vents. According to this model, the flow through the vent is always uni-directional, i.e., for any Δp

$$\dot{V}_H = \dot{V}_{H,ST} = C_D A_V (2\Delta p/\rho_H)^{1/2}; \quad \dot{V}_L = \dot{V}_{L,ST} = 0 \qquad (4)$$

where: $\dot{V}_H$ and $\dot{V}_L$ are volume flow rates through the vent from the high- to low-pressure and from the low- to high-pressure side of the vent, respectively; A_V is vent area; and Eq. (4) provides flow rates for the STANDARD model (subscript ST). This flow description seems reasonable, except it will always predict, incorrectly, that there will be uni-directional flow when $\Delta p \neq 0$, and that the flow is zero when $\Delta p = 0$.

To illustrate this, consider a condition of near-zero Δp, and assume that $\rho_T > \rho_B$, e.g., the vent joins a relatively high-temperature, small-density environment below from a relatively low-temperature, high-density environment above. This condition is one involving a state of hydrodynamic instability, where a two-directional exchange flow develops and a uni-directional description of the flow is always invalid.

The Mixed Flow Regime

The relevant fluid-dynamic instability for an unbounded interface has been studied theoretically by Taylor [1]. For the

unstable configuration and for $\Delta p = 0$, Epstein [2] established a correlation of exchange flow rate data from salt-/fresh-water exchange-flow experiments and Brown [3] established heat transfer correlations of data from analogous hot-air/cold-air exchange-flow experiments.

For any unstable arrangement of densities, if $|\Delta p|$ is small enough there will be a bi-directional or exchange flow though the vent. However, if $|\Delta p|$ is large enough the vent flow will be uni-directional. Indeed, there will always be a value $\Delta p = \Delta p_{FL}$, denoted as the critical or flooding value of Δp, which separates a uni-directional or *flooding* flow regime (for $\Delta p \geq \Delta p_{FL}$), where $\dot{V}_L = 0$, from a *mixed* flow regime ($0 \leq \Delta p < \Delta p_{FL}$), where $\dot{V}_L = \dot{V}_{EX} > 0$. $\dot{V}_{EX}$ is the above-mentioned *exchange flow*. Also, associated with any particular Δp_{FL} value is a corresponding volumetric flooding flow rate. This is denoted by $\dot{V}_{FL}$.

Epstein and Kenton [4] extended the work of Epstein [2] to $\Delta p \neq 0$. They studied the mixed flow regime with salt-/fresh-water experiments, measuring flow rates and $\dot{V}_{FL}$, but not Δp. Tan and Jaluria [5] carried out similar experiments, measuring Δp directly. However, the major focus here will be on turbulent, large-Gr flows, and, as will be shown, it seems that the latter experiments, carried out with relatively small-D (D $\leq$ 0.0127m) vents, were in the laminar- or transition-flow range.

Let $\dot{V}_N$ denote the net volume flow rate from the high- to the low-pressure side of the vent.

$$\dot{V}_N = \dot{V}_H - \dot{V}_L = \dot{V}_H - \dot{V}_{EX} \geq 0 \qquad (5)$$

This is the forced or pressure-driven part of the flow. At the two extremes of the mixed flow regime, $\dot{V}_N = \dot{V}_{FL}$ at $\Delta p = \Delta p_{FL}$ and $\dot{V}_N = 0$ at $\Delta p = 0$. Similarly, $\dot{V}_{EX}$, the buoyancy-driven part of the flow, reachs its maximum value, $\dot{V}_{EX,MX}$, at $\Delta p = 0$ and is zero at $\Delta p = \Delta p_{FL}$.

In view of the above, the standard model vent flow description of Eq. (4) must be modified as follows: There is a mixed flow regime, defined by $0 \leq \Delta p \leq \Delta p_{FL}$, where $\dot{V}_L = \dot{V}_{EX} \geq 0$. In this regime

$$\dot{V}_H(\Delta p = 0) = \dot{V}_{EX,MX} \leq \dot{V}_H \leq \dot{V}_H(\Delta p = \Delta p_{FL}) = \dot{V}_{FL} \qquad (6)$$

$$\dot{V}_L(\Delta p = \Delta p_{FL}) = 0 \leq \dot{V}_L \leq \dot{V}_L(\Delta p = 0) = \dot{V}_{EX,MX} \qquad (7)$$

The Uni-directional Flow Regime and the Significant Dependence of C_D on Relative Buoyancy

In addition to the difficulties of using the standard flow model in the mixed flow regime, there is also a problem in the uni-directional flow regime. In particular, use of a fixed value for C_D, denoted here as $C_{D,\infty}$ and associated with the orifice coefficient for high-Re flows through an orifice joining two regions of like fluids (see Perry [6]), is generally invalid.

Using fire-generated hot-/cold-air experiments and unstable horizontal vent configurations with high pressure at the top, it has been shown by Heskastad and Spaulding [7] that, until $\Delta p \gg \Delta p_{FL}$, there is a significant dependence of C_D on the relative buoyancy of the cross-vent environments, where $C_{D,FL}$, the value of C_D at the flooding condition, was measured to only

2

be of the order of a few tenths.

The fact that there is a difference between C_D for stable and unstable configurations is not suprising. For example, consider expected differences in the entrance flow near the vent, and their effects on C_D, for the two cases: 1) a less-dense fluid below penetrating a more-dense-fluid above (unstable) and 2) a more-dense fluid below penetrating a less-dense fluid above (stable). In the former case, the entering fluid will tend to rise from the vent to the upper space in a buoyant plume, whereas in the latter case the entering fluid will rise to a maximum elevation, move outward and downward to the bottom of the upper space, and continue its outward movement there, away from the vent opening, as a radial "floor jet."

For *shallow* (i.e., small L/D) circular vents of length L, the L/D = 0.011 data of Heskestad and Spaulding [7] indicate a smooth dependence of C_D on the relative buoyancy as expressed by Froude number (below, subscript HS refers to the names of the authors of [7]). From these data and from other considerations, Heskestad and Spaulding [7] conclude that for *uni-directional* flow

$$C_{D,HS} = C_{D,HS}(Fr_{HS}, Gr_{HS}); \quad \lim_{Fr_{HS} \to \infty} C_{D,HS} = C_{D,\infty} \quad (8)$$

$$Fr_{HS} = (\dot{V}_H/A_V)/[2gD(\rho_T - \rho_B)/\rho_T]^{1/2};$$
$$Gr_{HS} = g\rho_T(\rho_T - \rho_B)D^3/\bar{\mu}^2 \quad (9)$$

$$\mu = \mu(T); \quad \bar{\mu} = \mu(\bar{T}); \quad \bar{T} = (T_T + T_B)/2 \quad (10)$$

Eq. (8) indicates a general dependence of $C_{D,HS}$ on Gr_{HS}. However, for the shallow circular-vent data of Heskestad and Spaulding [7] (Gr_{HS} of the order of 10^7), $C_{D,HS}$ was in fact insensitive to changes in Gr_{HS} and no systematic variation of $C_{D,HS}$ on Gr_{HS} was observed. Beside determining the dependence of $C_{D,HS}$ on Fr_{HS}, Heskestad and Spaulding [7] also determined the flooding Froude number, Fr_{FL}, associated with measured values of $\dot{V}_{FL}$. For shallow circular vents, these results will be seen below to augment the previously mentioned analogous results of Epstein [2].

Results of Heskestad and Spaulding [7] include limited data on each of several vent designs other than shallow circular vents. These data indicate that orifice coefficient representations analogous to Eq. (8) can likely be established for vent designs other then shallow circular vents. In this regard, reliable results will require additional testing.

Representating Flow Rates as Explicit Functions of Δp

The objective of this work is to obtain a general model for the uni-directional and mixed flow regimes in unstable configurations where the high pressure is either at the top or the bottom. A desired characteristic of the model is that it predict flow rates as a function of Δp. As mentioned, the Heskestad and Spaulding [7] study provided data for flow rate vs Δp, but only for uni-directional flow with high pressure at the top. Also, in the mixed flow regime, flow rates, but not Δp were measured
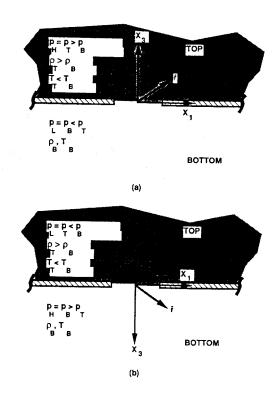

FIGURE 2. (a) CONFIGURATION 1 AND (b) CONFIGURATION 2 ILLUSTRATING CONDITIONS ASSOCIATED WITH BOUNDARY VALUE PROBLEMS 1 AND 2, RESPECTIVELY.

by Epstein and Kenton [4]. To establish the desired dependence of flow on Δp for the mixed flow regime, other considerations will be required in addition to the data.

The development of the flow model will be based on theoretical considerations of the relevant boundary value problems and on the above-mentioned data. Theoretical considerations will be presented in the next section. Following this, the sequence of model development will be: establish estimates for the onset of uni-directional flow, i.e., the flooding flow conditions; complete the model for the uni-directional flow regime; and develop the model for the mixed flow regime.

FLOW DYNAMICS FOR UNSTABLE CONFIGURATIONS: THEORETICAL CONSIDERATIONS

An unstable configuration with $p_T = p_H > p_B = p_L$, i.e., net flow from top to bottom, is designated as Configuration 1. Similarly, an unstable configuration, but with $p_B = p_H > p_T = p_L$, i.e., net flow from bottom to top, is designated as Configuration 2. Both configurations are sketched in Figure 2.

The Boundary Value Problems

The boundary value problems associated with Configurations 1 and 2 are identified as Problems 1 and 2, respectively. Assume that the fluid media in the top and bottom spaces are the same ideal gas. Then, in view of Eq. (2) the equation of

state for the gas can be approximated by

$$\rho T = \text{constant} = \rho_T T_T = \rho_B T_B = \bar{p}/R \tag{11}$$

where R is the gas constant and temperatures T_T and T_B correspond to specified ρ_T and ρ_B through Eq. (11). With the constraint of Eq. (3), Eq. (11) leads to the expected result

$$\Delta T = T_B - T_T > 0 \tag{12}$$

Eq. (11) will be a good approximation if

$$\Delta \rho g |X_3|/\bar{p} << 1 \text{ throughout the region of interest} \tag{13}$$

where Eq. (13) is always satisfied in practical problems, e.g., ventilated heated/cooled spaces and smoke spread (i.e., fire-heated/-contaminated air) during fires in multi-room facilities.

Designate the dependent variables velocity, pressure, density, and temperature for Problem N, N = 1 or 2, as $U_i^{(N)}$, $p^{(N)}$, $\rho^{(N)}$, and $T^{(N)}$, respectively. Then, through the equations of conservation of mass, momentum (i.e., the Navier Stokes equations), energy, and the modified equation of state, Eq. (12), and for the specified parameters (which determine the boundary conditions), all of these variables are functions of the co-ordinates, $X_i^{(N)}$, and the temperature-dependent material properties: $C_p(T)$, specific heat at constant pressure; k(T), thermal conductivity; and $\mu(T)$.

Problems 1 and 2 can be put in dimensionless form by introducing the following dimensionless dependent variables

Problem 1:

$$U_i^{*(1)} = U_i^{(1)}/(2gD\varepsilon)^{1/2}; \quad p^{*\prime(1)} = (p - \bar{p} + g\bar{\rho}X_3)/(2g\Delta\rho D);$$

$$\rho^{*\prime(1)} = (\rho/\bar{\rho} - 1)/\varepsilon; \quad T^{*\prime(1)} = (1 - T/\bar{T})/\varepsilon \tag{14}$$

Problem 2:

$$U_i^{*(2)} = U_i^{(2)}/(2gD\varepsilon)^{1/2}; \quad p^{*\prime(2)} = (p - \bar{p} - g\bar{\rho}X_3)/(2g\Delta\rho D);$$

$$\rho^{*\prime(2)} = (1 - \rho/\bar{\rho})/\varepsilon; \quad T^{*\prime(2)} = (T/\bar{T} - 1)/\varepsilon$$

Neglecting pdV work and viscous dissipation in the energy equation it has been shown by Cooper [8] that the variables of Eq. (14) are functions only of $X_i^{*(N)}$ and the parameters ε, Π, $\bar{Gr}$, and $\bar{Pr}$ where[1]

---

[1] Since $\varepsilon > 0$, the absolute value designation for ε is unnecessary here. However, it will be useful in later applications of Eq. (15). A similar note is relevant below in the presentation of Eqs. (41) and (47).

$$X_i^{*(N)} = X_i^{(N)}/D; \quad \varepsilon = \Delta\rho/\bar{\rho} = \Delta T/\bar{T} < 2; \quad \bar{\rho} = (\rho_T + \rho_B)/2$$

$$\Pi = \Delta p/(4g\Delta\rho D); \quad \bar{Gr} = 2gD^3|\varepsilon|/[\mu(\bar{T})/\bar{\rho}]^2; \tag{15}$$

$$\bar{Pr} = C_p(\bar{T})\mu(\bar{T})/k(\bar{T})$$

Thus, for example,

$$U_i^{*(N)} = U_i^{*(N)}(X_i^{*(N)}; \Pi, \varepsilon, \bar{Gr}, \bar{Pr}) \tag{16}$$

In addition, it has been shown by Cooper [8] that replacing ε by $-\varepsilon$ in Problem 1 leads to Problem 2, and replacing ε by $-\varepsilon$ in Problem 2 leads to Problem 1.

Now assume that solutions to Problems 1 and 2 exist for both negative and positive ε. Note that there is no *a priori* reason to suspect that solutions for $\varepsilon < 0$ for either problem are physically meaningful. However, because of the above-stated relationship between the N = 1 and 2 boundary value problems, it is evident that a general solution to one of these, including results for both positive and negative ε, provides the general solution to the physical problem of the other, i.e., for $\varepsilon > 0$. Thus, for example,

$$U_i^{*(1)}(X_i^{*(1)}; \Pi, \overset{+}{\underset{-}{}}\varepsilon, \bar{Gr}, \bar{Pr}) = U_i^{*(2)}(X_i^{*(2)}; \Pi, \overset{-}{\underset{+}{}}\varepsilon, \bar{Gr}, \bar{Pr}) \tag{17}$$

where similar equations can be written for the $p^{*\prime(N)}$, $\rho^{*\prime(N)}$, and $T^{*\prime(N)}$. Eq. (17) will used below to determine and extend relationships between results of Configuration-1- and 2-type experiments.

Dimensionless Volume Flow Rates

For N = 1 or 2, $\dot{V}_H^{(N)}$ and $\dot{V}_L^{(N)}$ would be calculated from

$$\dot{V}_H^{(N)} = \int_{A_V} \sigma_H^{(N)}(X_3^{(N)} = 0)dA_V;$$

$$\sigma_H^{(N)}(U_3^{(N)}) = \begin{cases} -U_3^{(N)} & \text{where } U_3^{(N)}(X_3^{(N)} = 0) < 0 \\ 0 & \text{where } U_3^{(N)}(X_3^{(N)} = 0) \geq 0 \end{cases} \tag{18}$$

$$\dot{V}_L^{(N)} = \int_{A_V} \sigma_L^{(N)}(X_3^{(N)} = 0)dA_V;$$

$$\sigma_L^{(N)}(U_3^{(N)}) = \begin{cases} U_3^{(N)} & \text{where } U_3^{(N)}(X_3^{(N)} = 0) > 0 \\ 0 & \text{where } U_3^{(N)}(X_3^{(N)} = 0) \leq 0 \end{cases}$$

For example, for *uni-directional* flow, when $\Pi \geq \Pi_{FL}$ corresponding to $\Delta p \geq \Delta p_{FL}$, Eqs. (18) become

$$\dot{V}_H^{(N)} = -\int_{A_V} U_3^{(N)}(X_3^{(N)} = 0)dA_V = -A_V\bar{U}_3^{(N)}; \quad \dot{V}_L^{(N)} = 0 \tag{19}$$

where the integral is over the entire area of the vent and $\bar{U}_3^{(N)}$ is the average value of $U_3^{(N)}$ at $X_3^{(N)} = 0$. Using Eqs. (16), the dimensionless version of Eq. (18) leads to the definition of $\bar{Fr}_H$

4

$$\bar{Fr}_H^{(N)} = (\dot{V}_H^{(N)}/A_V)/(2gD\varepsilon)^{1/2} = -\dot{U}_3^{*(N)} \qquad (20)$$

$$= -\left[\int\limits_{A_V} U_3^{*(N)}(X_3^{*(N)} = 0; \Pi, \varepsilon, \bar{Gr})d(A_V/D^2)\right]/(A_V/D^2)$$

In a similar way, carrying out the above proceedure on Eqs. (18) for the *mixed flow* regime leads to

$$\bar{Fr}_H^{(N)}(\Pi, \varepsilon, \bar{Gr}, \bar{Pr}) = (\dot{V}_H^{(N)}/A_V)/(2gD\varepsilon)^{1/2};$$

$$\bar{Fr}_L^{(N)}(\Pi, \varepsilon, \bar{Gr}, \bar{Pr}) = (\dot{V}_L^{(N)}/A_V)/(2gD\varepsilon)^{1/2} \qquad (21)$$

Also, using the result of Eq. (17) leads to

$$\bar{Fr}_H^{(N)}(\Pi, \pm\varepsilon, \bar{Gr}, \bar{Pr}) = \bar{Fr}_H^{(N)}(\Pi, \mp\varepsilon, \bar{Gr}, \bar{Pr});$$

$$\bar{Fr}_L^{(N)}(\Pi, \pm\varepsilon, \bar{Gr}, \bar{Pr}) = \bar{Fr}_L^{(N)}(\Pi, \mp\varepsilon, \bar{Gr}, \bar{Pr}) \qquad (22)$$

UNI-DIRECTIONAL FLOW

The Flow Coefficient and the Large-Gr Assumption

The C_D definition remains useful for uni-directional flow. Using Eqs. (15) and (21) in Eq. (4) leads to

$$C_D^{(N)} = [(\rho_H/\bar{\rho})/(4\Pi)]^{1/2}\bar{Fr}_H^{(N)}; \quad \lim_{\bar{Fr}_H^{(N)} \to \infty} C_D^{(N)} = C_{D,\infty};$$

$$\rho_H/\bar{\rho} = \begin{vmatrix} 1 + \varepsilon/2 \text{ for } N = 1 \\ 1 - \varepsilon/2 \text{ for } N = 2 \end{vmatrix} \qquad (23)$$

and Eqs. (21)-(23) lead to

$$C_D^{(N)} = C_D^{(N)}(\Pi, \varepsilon, \bar{Gr}, \bar{Pr});$$

$$C_D^{(1)}(\Pi, \pm\varepsilon, \bar{Gr}, \bar{Pr}) = C_D^{(2)}(\Pi, \mp\varepsilon, \bar{Gr}, \bar{Pr}) \qquad (24)$$

Note that C_D is for a particular vent design and would generally vary from one design to another, e.g., for shallow circular vents vs shallow square vents. **UNLESS NOTED OTHERWISE, THE REMAINDER OF THIS WORK FOCUSES ONLY ON TURBULENT, LARGE-GR FLOW THROUGH SMALL-L/D CIRCULAR VENTS,** where "small-L/D" means, approximately, L/D < 0.10, and where the "large-Gr" terminology will be clarified below.

The Flooding Condition

The Region of Turbulent, Large-Gr Flow. For fixed ε, $\bar{Gr}$, and $\bar{Pr}$ there is a specific Π, associated with Δp_{FL} and depending on N, that leads to flooding. This is designated as $\Pi_{FL}^{(N)}$, where

$$\Pi_{FL}^{(N)}(\varepsilon, \bar{Gr}, \bar{Pr}) \equiv \Delta p_{FL}^{(N)}/(4g\Delta\rho D);$$

$$\Pi_{FL}^{(1)}(\pm\varepsilon, \bar{Gr}, \bar{Pr}) = \Pi_{FL}^{(2)}(\mp\varepsilon, \bar{Gr}, \bar{Pr}) \qquad (25)$$

and where the corresponding values $\bar{Fr}_{H,FL}^{(N)}$, $\dot{V}_{H,FL}^{(N)}$, and

$C_{D,FL}^{(N)}$ are

$$\bar{Fr}_{H,FL}^{(N)}(\varepsilon, \bar{Gr}, \bar{Pr}) = \bar{Fr}_H^{(N)}(\Pi_{FL}^{(N)}, \varepsilon, \bar{Gr}, \bar{Pr})$$

$$= (\dot{V}_{H,FL}^{(N)}/A_V)/(2gD\varepsilon)^{1/2} \qquad (26)$$

$$C_{D,FL}^{(N)}(\varepsilon, \bar{Gr}, \bar{Pr}) = C_D^{(N)}(\Pi_{FL}^{(N)}, \varepsilon, \bar{Gr}, \bar{Pr}) \qquad (27)$$

Also, from Eq. (23) and from Eqs. (25)-(27)

$$C_{D,FL}^{(1)} = [(1 + \varepsilon/2)/(4\Pi_{FL}^{(1)})]^{1/2}\bar{Fr}_{H,FL}^{(1)};$$

$$C_{D,FL}^{(2)} = [(1 - \varepsilon/2)/(4\Pi_{FL}^{(2)})]^{1/2}\bar{Fr}_{H,FL}^{(2)} \qquad (28)$$

$$\bar{Fr}_{H,FL}^{(1)}(\pm\varepsilon, \bar{Gr}, \bar{Pr}) = \bar{Fr}_{H,FL}^{(2)}(\mp\varepsilon, \bar{Gr}, \bar{Pr});$$

$$C_{D,FL}^{(1)}(\pm\varepsilon, \bar{Gr}, \bar{Pr}) = C_{D,FL}^{(2)}(\mp\varepsilon, \bar{Gr}, \bar{Pr}) \qquad (29)$$

Heskestad and Spaulding [7] present data from Configuration-1 experiments with air ($\bar{Pr} = 0.7$) in the uni-directional flow regime. $\bar{Fr}$, Π, ε, and $\bar{Gr}$ corresponding to their data are presented in Table 1. As indicated, of the 13 data points, the first 6 are associated with the flooding condition. [The above theoretical analysis is for perfect gas media and is valid for the entire range - 2 < ε < 2. However, for $|\varepsilon| \ll 1$, when the Bousinesque approximation is applicable, there is an analogy between Figure-1-type problems involving perfect gases and incompressible or nearly incompressible liquids. In the case of small-ε problems involving liquids, buoyancy effects which drive the exchange flows can be the result of temperature differences or of concentration differences of a solvent. This is the justification for use of the salt-/fresh-water data (where $|\varepsilon| < 0.2$) of Epstein and Kenton [4], Tan and Jaluria [5], and Heskestad and Spaulding [7] in the data analyses to follow.]

Flooding conditions were measured in the salt-/fresh-water experiments ($\bar{Pr} \approx 7$) of Epstein and Kenton [4] and Tan and Jaluria [5]. All small-L/D flooding data from Epstein and Kenton [4], Tan and Jaluria [5], and Heskestad and Spaulding [7] are presented in Table 2. As indicated in the table, the salt-water experiments involved both Configurations 1 (referred to by Epstein and Kenton [4] as "draining" experiments) and 2 (referred to in [4] as "injection" experiments). Since Δp was not measured by Epstein and Kenton [4], Π and $C_{D,FL}^{(N)}$ are not available for their data.

For the above data, $\bar{Fr}_{H,FL}^{(N)}(\bar{Gr})$, as plotted in Figure 3, is seen to be relatively insensitive to changes in $\bar{Gr}$ in the range $2.99(10^7) \le \bar{Gr} \le 2.91(10^8)$. (As will be explained below, in this range the observed variations in $\bar{Fr}_{H,FL}^{(N)}$ are primarily a result of its dependence on ε.) However, there is a significant increase in $\bar{Fr}_{H,FL}^{(N)}$, over the larger-$\bar{Gr}$ values, for $\bar{Gr} \le 1.42(10^7)$, i.e., for the data of Tan and Jaluria [5]. Using flooding data for square, rectangular, and circular vents, acquired over a large range of $\bar{Gr}$, Figure 10 of Heskestad and Spaulding [7] indicates a similar insensitivity in the dependence of $\bar{Fr}_{H,FL}^{(N)}$ on $\bar{Gr}$ for $\bar{Gr} > 2(10^7)$ and a similar, relatively-

Test[1]	ε	$\overline{Fr}_H^{(1)}$	Π	$C_D^{(1)}$	$\overline{Gr}$[6]	$\overline{Fr}_H^{(1)}/\overline{Fr}_{H,FL}^{(1)}$ [5]	$C_D^{(1)}/C_{D,\infty}$ [5]	$\Pi/\Pi_{FL}^{(1)}$ [5]
54[2]	0.521	0.216	0.601	0.156	$2.99(10^7)$	0.924	0.261	1.10
55[2]	0.559	0.243	0.532	0.188	$3.49(10^7)$	1.02	0.314	0.923
56[2]	0.282	0.186	0.467	0.146	$4.64(10^7)$	0.910	0.243	1.24
59[2]	0.373	0.227	0.392	0.198	$4.74(10^7)$	1.05	0.329	0.901
60[2]	0.474	0.238	0.456	0.196	$4.06(10^7)$	1.04	0.326	0.900
61[2]	0.260	0.248	0.382	0.214	$4.66(10^7)$	1.23	0.356	1.04
53[3]	0.521	0.257	0.657	0.178	$2.99(10^7)$	1.10	0.296	1.21
53[3,4]	0.521	0.474	0.708	0.316	$2.99(10^7)$	2.03	0.527	1.30
53[3,4]	0.521	0.661	0.848	0.403	$2.99(10^7)$	2.83	0.671	1.56
53[3,4]	0.521	0.814	0.111	0.434	$2.99(10^7)$	3.48	0.723	2.04
54[4]	0.521	0.461	0.631	0.326	$2.99(10^7)$	1.97	0.543	1.16
55[4]	0.559	0.262	0.455	0.219	$3.49(10^7)$	1.10	0.366	0.790
56[4]	0.282	0.342	0.603	0.235	$4.64(10^7)$	1.67	0.392	1.59

{1}	See TABLES III and VI of Heskestad and Spaulding [7].
{2}	Identified by Heskestad and Spaulding [7] as the flooding condition, i.e., the $\overline{Fr}_H^{(1)}$, Π, and $C_D^{(1)}$ values for this datum point are $\overline{Fr}_{H,FL}^{(1)}$, $\Pi_{FL}^{(1)}$, and $C_{D,FL}^{(1)}$, respectively.
{3}	Same fuel and fuel flow rate as Test Condition 54.
{4}	T_T and T_B are not presented by Heskestad and Spaulding [7]; it is assumed here that the values of these were the same as the values measured in the same test, i.e., the same fuel and fuel flow rate, but at flooding conditions.
{5}	$C_{D,\infty}$ is from Eq. (36); $\overline{Fr}_{H,FL}^{(1)} = \overline{Fr}_{H,FL}^{(1)}(\varepsilon, \overline{Gr} \to \infty)$ and $\Pi_{FL}^{(1)} = \Pi_{FL}^{(1)}(\varepsilon, \overline{Gr} \to \infty)$ are calculated from Eqs. (31)-(33).
{6}	In calculating $\overline{Gr}$ from Eq. (15), the kinematic viscosity, $\nu(\overline{T}) = \mu(\overline{T})/\rho$, determined from Hilsenrath [9]

$$\nu(T) = [0.04128(T/K)^{5/2}(10^{-7})/(T/K + 110.4)]m^2/s$$

TABLE 1. RESULTS DERIVED FROM THE CONFIGURATION-1 EXPERIMENTAL DATA OF HESKASTAD AND SPAULDING [7] FOR FLOW THROUGH A D = 0.153m, L/D = 0.011 CIRCULAR VENT, AND FROM EQS. (31) AND (32') FOR $\overline{Fr}_{H,FL}^{(1)}$ AND $\Pi_{FL}^{(1)}$.

Reference Number	ε	Configuration Number	$\overline{Fr}_{H,FL}^{(1)}$	$\overline{Gr}$	$C_{D,FL}^{(1)}$	$\Pi_{FL}^{(1)}$
[7]	0.521	1	0.216	$2.99(10^7)$	0.156	0.601
[7]	0.559	1	0.243	$3.49(10^7)$	0.188	0.532
[7]	0.282	1	0.186	$4.64(10^7)$	0.146	0.467
[7]	0.373	1	0.227	$4.74(10^7)$	0.198	0.392
[7]	0.474	1	0.238	$4.06(10^7)$	0.196	0.456
[7]	0.260	1	0.248	$4.66(10^7)$	0.214	0.382
[4]	0.1426	1	0.1917	$5.31(10^7)$	{1}	{1}
[4]	0.1410	1	0.1755	$5.25(10^7)$	{1}	{1}
[4]	0.1378	2	0.1632	$5.13(10^7)$	{1}	{1}
[4]	0.1487	1	0.2057	$5.54(10^7)$	{1}	{1}
[4]	0.1339	2	0.1783	$4.98(10^7)$	{1}	{1}
[4]	0.1456	1	0.1826	$2.91(10^8)$	{1}	{1}
[4]	0.1329	1	0.1709	$2.66(10^8)$	{1}	{1}
[4]	0.1417	1	0.1618	$2.84(10^8)$	{1}	{1}
[5]	0.0469	2	0.2534	$4.28(10^6)$	0.0966	1.638
[5]	0.0658	2	0.4383	$6.00(10^6)$	0.194	1.191
[5]	0.0898	2	0.3463	$8.20(10^6)$	0.168	0.970
[5]	0.1208	2	0.4132	$1.10(10^7)$	0.218	0.793
[5]	0.1550	2	0.3877	$1.41(10^7)$	0.220	0.659

{1}	This value is not available since Δp was not measured.

TABLE 2. SMALL-L/D DATA ON FLOODING CONDITIONS FROM EPSTEIN AND KENTON [4], TAN AND JALURIA [5], AND HESKESTAD AND SPAULDING [7].

abrupt increase in $\overline{Fr}_{H,FL}^{(N)}$ as $\overline{Gr}$ drops below approximately $2(10^7)$. (In computing $\overline{Gr}$ for the square- and rectangular-vent data of Heskestad and Spaulding [7], Eq. (15) was used, where D is replaced by the width of the vent. Of these data, the one with the largest $\overline{Gr} = 1.54(10^{10})$, is for flooding flow through a

rectangular vent of dimension 2.03mx0.91m.)

Consistent with the above observation, it is assumed that in the present problem, $\overline{Gr} > 2(10^7)$ defines a range of turbulent, buoyancy-driven, free-flow phenomena where the $\overline{Gr}$-depen
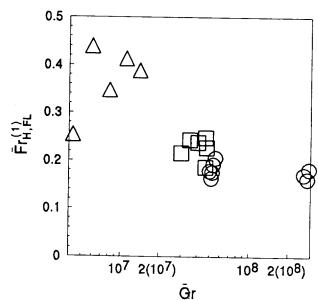

FIGURE 3. PLOT OF $\overline{Fr}_{H,FL}^{(1)}$ AS A FUNCTION OF $\overline{Gr}$ FOR ALL SMALL-L/D DATA OF TABLE 2 (O - EPSTEIN AND KENTON [4]; Δ - TAN AND JALURIA [5]; □ - HESKESTAD AND SPAULDING [7]).

dence of the boundary value problem is generally negligible.

The above discussion ignores the $\bar{Pr}$-dependence of $\bar{Fr}_{H,FL}^{(N)}$. Here it is reasonable to assume that in the large-$\bar{Gr}$ range of practical interest, molecular diffusion effects of $\bar{Pr}$ variations are negligible, at least for the approximate range $0.7 \leq \bar{Pr} \leq 7$.

In view of the above, for large enough $\bar{Gr}$ it is assumed that $\bar{Fr}_H^{(N)}$, $\bar{Fr}_L^{(N)}$, and $C_D^{(N)}$ are functions of Π and ε, and that $\bar{Fr}_{H,FL}^{(N)}$, $C_{D,FL}^{(N)}$, and $\Pi_{FL}^{(N)}$ are only functions of ε, i.e.,

For $\bar{Gr} > 2(10^7)$: $\bar{Fr}_{H,FL}^{(N)}(\varepsilon, \bar{Gr}, \bar{Pr}) = \bar{Fr}_{H,FL}^{(N)}(\varepsilon)$;

$$\bar{Fr}_H^{(N)}(\Pi, \varepsilon, \bar{Gr}, \bar{Pr}) = \bar{Fr}_H^{(N)}(\Pi, \varepsilon); \text{ etc.} \quad (30)$$

The Eq.-(30) assumption will also be adopted below in the mixed flow regime. In contrast to this, it is assumed that $\bar{Gr} < 2(10^7)$ defines transition and laminar flow regimes of the problem, where $\bar{Gr}$- and possible $\bar{Pr}$-dependence is important.

Practical vent flow problems of the type of interest here, e.g., problems related to fire safety and building ventilation, are typically confined to the large-$\bar{Gr}$ range, $\bar{Gr} > 2(10^7)$. **THE REMAINDER OF THIS WORK FOCUSES ONLY ON LARGE-GR PROBLEMS, AND, UNLESS NOTED OTHERWISE, GR- AND PR-INDEPENDENCE OF ALL THE FLOW PHENOMENA IS ALWAYS ASSUMED.**

The Functions $Fr_{H,FL}^{(N)}(\varepsilon)$, $\Pi_{FL}^{(N)}(\varepsilon)$, and $C_{D,FL}^{(N)}(\varepsilon)$. The $\bar{Fr}_{H,FL}^{(1)}(\varepsilon)$, $\Pi_{FL}^{(1)}(\varepsilon)$, and $C_{D,FL}^{(1)}(\varepsilon)$ data of Table 2 from Epstein and Kenton [4] and Heskestad and Spaulding [7] are plotted in Figures 4, 5, and 6, respectively. [Tan and Jaluria [5] data do not satisfy the large-$\bar{Gr}$ criterion of Eq. (30).] In the plots, the reciprocal properties of Eqs. (25) and (29) are implemented. Thus, the data and solution are plotted in terms of the Configu-
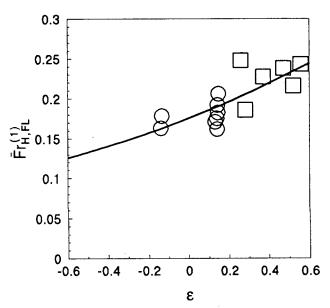
ration-1 problem, with Configuration-2 results presented with $\varepsilon < 0$. Also plotted in Figure 4 is the following least-squares fit (with proper analytic characteristics) of the $\bar{Fr}_{H,FL}^{(1)}(\varepsilon)$ data.

$$\bar{Fr}_{H,FL}^{(1)}(\varepsilon) = 0.1754\exp(0.5536\varepsilon) \quad (31)$$

As seen in Figure 6, $C_{D,FL}^{(1)}$ data are very sparse, with no entries for small $|\varepsilon|$ or $\varepsilon < 0$. Also, the data scatter does not provide qualitative insight on the "shape" of the $C_{D,FL}^{(1)}$ function. Until
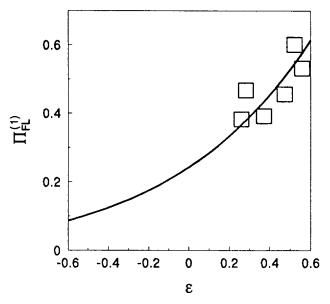
FIGURE 5. PLOT OF THE $\Pi_{FL}^{(1)}(\varepsilon)$: DATA OF TABLE 2; ——, LEAST-SQUARES CURVE FIT OF EQ. (38').
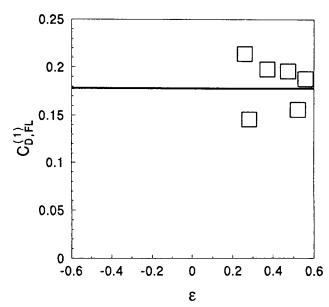
FIGURE 4. PLOT OF $\bar{Fr}_{H,FL}^{(1)}(\varepsilon)$: DATA OF TABLE 2 (O - EPSTEIN AND KENTON [4], □ - HESKESTAD AND SPAULDING [7]); ——, LEAST-SQUARES CURVE FIT OF EQ. (36).

FIGURE 6. PLOT OF $C_{D,FL}^{(1)}(\varepsilon)$: □, DATA OF TABLE 2; ——, CURVE FIT OF EQ. (33).

more data becomes available, it is therefore reasonable to approximate $C_{D,FL}^{(1)}(\varepsilon)$ as a constant. A possible choice is the average value, 0.1830. However, since C_D is derived from Eq. (4), and since the $C_{D,FL}^{(1)}$ entries of Table 2 are derived from the $Fr_{H,FL}^{(1)}(\varepsilon)$ and $\Pi_{FL}^{(1)}(\varepsilon)$ data according to Eq. (28), a more appropriate, constant, representative value for $C_{D,FL}^{(N)}$ is one that provides a least squares fit of the $\Pi_{FL}^{(1)}(\varepsilon)$ data. From Eq. (28)

$$\Pi_{FL}^{(1)}(\varepsilon) = (1 + \varepsilon/2)[\overline{Fr}_{H,FL}^{(1)}(\varepsilon)/C_{D,FL}^{(1)}]^2/4 \qquad (32)$$

Using Eq. (31) in Eq. (32), it was found that

$$C_{D,FL}^{(1)}(\varepsilon) = 0.1780 \qquad (33)$$

provides the least squares fit to the $\Pi_{FL}^{(1)}(\varepsilon)$ data of Table 2. Eq. (25), and Eqs. (31) and (33) in Eq. (32) lead to

$$\Pi_{FL}^{(1)}(\varepsilon) = \Delta p_{FL}^{(1)}/(4g\Delta\rho D) = 0.2427(1 + \varepsilon/2)\exp(1.1072\varepsilon) \qquad (32')$$

Eq. (32') is plotted in Figure 5 and Eq. (33) is plotted in Figure 6.

In Figure 5, the sparseness of the available $\Pi_{FL}^{(1)}(\varepsilon)$ data, especially with the absence of entries for small $|\varepsilon|$ or $\varepsilon < 0$, and the predicted significant $\Pi_{FL}^{(1)}(\varepsilon)$-variation of Eq. (32') in the ε-range of interest, is problematic. Nevertheless, the results of Eqs. (31)-(33) are plausible, and they fill a gap where alternative choices are not available. These results will be used throughout the remainder of this work.

An Estimate for C_D

It is convenient to normalize Eq. (23) as follows

$$C_D^{(1)}(\Pi, \varepsilon)/C_{D,\infty} = \qquad (34)$$

$$[C_{D,FL}^{(1)}(\varepsilon)/C_{D,\infty}][\overline{Fr}_H^{(1)}(\Pi, \varepsilon)/\overline{Fr}_{H,FL}^{(1)}(\varepsilon)]/[\Pi/\Pi_{FL}^{(1)}(\varepsilon)]^{1/2}$$

For uni-directional flow, $\Pi/\Pi_{FL}^{(N)}(\varepsilon) \geq 1$, where, independent of ε, the limit $\Pi/\Pi_{FL}^{(N)}(\varepsilon) \to \infty$ leads to the standard Bernoulli orifice flow condition, i.e.,

$$\lim_{\Pi/\Pi_{FL}^{(1)}(\varepsilon) \to 1} C_D^{(1)}(\Pi, \varepsilon)/C_{D,\infty} = [C_{D,FL}^{(1)}(\varepsilon)/C_{D,\infty}] \equiv 1/\sigma_1(\varepsilon);$$

$$\lim_{\Pi/\Pi_{FL}^{(1)}(\varepsilon) \to \infty} C_D^{(1)}(\Pi, \varepsilon)/C_{D,\infty} = 1 \qquad (35)$$

and where $C_{D,\infty}$ is taken to be the value associated with sharp-edged orifices and slots (Perry [6])

$$C_{D,\infty} = 0.60 \qquad (36)$$

To obtain vent flow rate as a function of Δp, it will be convenient to choose the functional form

$$\overline{Fr}_H^{(1)}/\overline{Fr}_{H,FL}^{(1)} = f(\Pi/\Pi_{FL}^{(1)}; \varepsilon) \qquad (37)$$

and to approximate $C_D^{(1)}(\Pi, \varepsilon)/C_{D,\infty}$ of Eq. (34) as

$$C_D^{(1)}(\Pi, \varepsilon)/C_{D,\infty} = \qquad (38)$$

$$(\overline{Fr}_H^{(1)}/\overline{Fr}_{H,FL}^{(1)})/\{[(\overline{Fr}_H^{(1)}/\overline{Fr}_{H,FL}^{(1)}) - 1 + \sigma_2^2]^2 + \sigma_1^2 - \sigma_2^4\}^{1/2}$$

where Eq. (38) satisfies Eqs. (35) and $\sigma_2 = \sigma_2(\varepsilon)$ would be determined from a fit of $C_D^{(1)}(\Pi, \varepsilon)/C_{D,\infty}$ data.

As can be seen from Table 1, except for $\varepsilon = 0.521$, $C_D^{(1)}/C_{D,\infty}$ data for non-flooding conditions are limited to single data points for each of $\varepsilon = 0.282$ and 0.559. Until further data are available it is therefore reasonable to approximate $\sigma_2(\varepsilon)$ as a constant. Using Eqs. (35) and (36) and the $C_{D,FL}^{(1)}$ approximation of Eq. (33), and choosing σ_2 as the value providing a least squares fit to all data of Table 1 leads to

$$\sigma_1(\varepsilon) = 0.60/0.1780 = 3.370; \quad \sigma_2(\varepsilon) = 1.045 \qquad (39)$$

$C_D^{(1)}(\Pi, \varepsilon)/C_{D,\infty}$ vs $\overline{Fr}_H^{(1)}/\overline{Fr}_{H,FL}^{(1)}$ data of Table 1 and Eqs. (38) and (39) are plotted in Figure 7.

The Model for the Vent Flow in the Uni-directional Flow Regime

Replacing the left side of Eq. (34) by the right side of Eq. (38) and solving for $\overline{Fr}_H^{(1)}/\overline{Fr}_{H,FL}^{(1)}$ leads to the desired result for predicting the vent flow rate in the uni-directional flow regime

For $\Delta p/\Delta p_{FL}^{(1)} = \Pi/\Pi_{FL}^{(1)} \geq 1$: $\qquad (40)$

$$\dot{V}_H^{(1)}/\dot{V}_{H,FL}^{(1)} = \overline{Fr}_H^{(1)}/\overline{Fr}_{H,FL}^{(1)}$$

$$= 1 - \sigma_2^2 + [\sigma_2^4 + \sigma_1^2(\Delta p/\Delta p_{FL}^{(1)} - 1)]^{1/2};$$

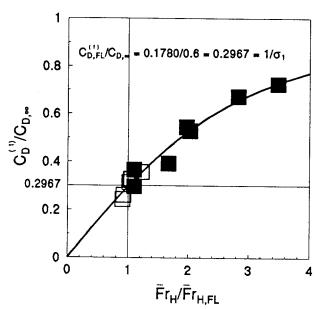$$\dot{V}_L^{(1)}/\dot{V}_{H,FL}^{(1)} = \overline{Fr}_L^{(1)}/\overline{Fr}_{H,FL}^{(1)} = 0$$

FIGURE 7. PLOT OF $C_D^{(1)}/C_{D,\infty}$ vs $Fr_H^{(1)}/Fr_{H,FL}^{(1)}$: ——, EQ. (43) AND (44); ■, NON-FLOODING DATA OF TABLE 1; □, FLOODING DATA OF TABLE 1.

where Eq. (39) gives σ_1 and σ_2, Eq. (32') gives $\Delta p_{FL}^{(1)}$, and Eqs. (26) and (31) lead to

$$\dot{V}_{H,FL}^{(1)} = 0.1754(2gD|\varepsilon|)^{1/2}A_V\exp(0.5536\varepsilon) \tag{41}$$

As required, Eq. (40) guarantees that $\dot{V}_H^{(1)}/\dot{V}_{H,FL}^{(1)}$ is a monotonically increasing function of $\Delta p/\Delta p_{FL}^{(1)}$ for $\Delta p/\Delta p_{FL}^{(1)} \geq 1$. [This is a consequence of the chosen form of Eq. (38).] Also, Eq. (40) satisfies the large-Δp limit, which is equivalent to the standard Bernoulli orifice flow condition, i.e.,

$$\lim_{\Delta p/\Delta p_{FL}^{(1)} \to \infty} \dot{V}_H^{(1)}/\dot{V}_{H,FL}^{(1)} = (C_{D,\infty}/C_{D,FL}^{(1)})(\Delta p/\Delta p_{FL}^{(1)})^{1/2} \tag{42}$$

Eq. (40) is the model equation result for the uni-directional flow regime. From this, a plot of $\dot{V}_H^{(1)}/\dot{V}_{H,FL}^{(1)}$ vs $\Delta p/\Delta p_{FL}^{(1)}$ is presented in Figure 8 together with plots of the Table-1 data and the Bernoulli-flow limit of Eq. (42). From the figure it can be seen that at the flooding condition the standard Bernoulli-flow equation over-estimates the expected flow rate by a factor in excess of 3, and that only after $\Delta p/\Delta p_{FL}^{(1)}$ exceeds 3 or 4 does the standard model provide flow-rate estimates correct to within a few tens of percent.

THE MIXED FLOW REGIME

Boundary Conditions for the Flow Components

For the mixed flow regime it is convenient to adopt the following approximate representations of $\dot{V}_N^{(1)}/\dot{V}_{H,FL}^{(1)}$ and $\dot{V}_L^{(1)}/\dot{V}_{H,FL}^{(1)}$. These are consistent with definitions and end-point conditions of Eqs. (5)-(7), and with a requirement of
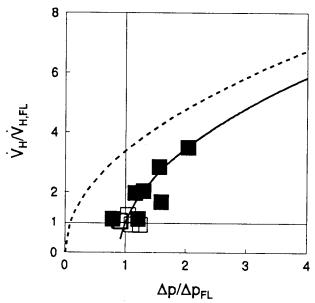

FIGURE 8. PLOT OF $\dot{V}_H^{(1)}/\dot{V}_{H,FL}^{(1)} = \bar{F}r_H^{(1)}/\bar{F}r_{H,FL}^{(1)}$ vs $\Delta p/\Delta p_{FL}^{(1)}$ $= \Pi/\Pi_{FL}^{(1)}$: ——, MODEL EQUATION FOR UNI-DIRECTIONAL FLOW REGIME, EQS. (44) AND (45); – – – , BERNOULLI FLOW LIMIT OF EQ (47); ■, NON-FLOODING DATA OF TABLE 1; □, FLOODING DATA OF TABLE 1.

continuity-of-slope (both $\dot{V}_N^{(1)}$ and $\dot{V}_H^{(1)}$ as functions of Δp) across the flooding limit boundary where, $\Delta p/\Delta p_{FL}^{(1)} = 1$.

$$\dot{V}_N^{(1)}/\dot{V}_{H,FL}^{(1)} = \{M - [1 + (M^2 - 1)(1 - \Delta p/\Delta p_{FL}^{(1)})]^{1/2}\}/(M - 1) \tag{43}$$

or

$$\Delta p/\Delta p_{FL}^{(1)} = - [(M - 1)/(M + 1)](\dot{V}_N^{(1)}/\dot{V}_{H,FL}^{(1)})^2 \tag{43'}$$
$$+ [2M/(M + 1)](\dot{V}_N^{(1)}/\dot{V}_{H,FL}^{(1)})$$

$$\dot{V}_L^{(1)}/\dot{V}_{H,FL}^{(1)} = \tag{44}$$

$$\dot{V}_{EX,MX}/\dot{V}_{H,FL}^{(1)}\{[1 + m_1(\dot{V}_{H,FL}^{(1)}/\dot{V}_{EX,MX})/2](1 - \Delta p/\Delta p_{FL}^{(1)})^2$$
$$- [2 + m_1(\dot{V}_{H,FL}^{(1)}/\dot{V}_{EX,MX})/2](1 - \Delta p/\Delta p_{FL}^{(1)})\}^2$$

or

$$\dot{V}_L^{(1)}/\dot{V}_{EX,MX} = \tag{44'}$$

$$[(1 + m_2/2)(1 - \Delta p/\Delta p_{FL}^{(1)})^2 - (2 + m_2/2)(1 - \Delta p/\Delta p_{FL}^{(1)})]^2$$

$$\dot{V}_H^{(1)}/\dot{V}_{H,FL}^{(1)} = \dot{V}_L^{(1)}/\dot{V}_{H,FL}^{(1)} + \dot{V}_N^{(1)}/\dot{V}_{H,FL}^{(1)} \tag{45}$$

$$M = 2m_1 - 1 = (\sigma_1/\sigma_2)^2 - 1 = 9.400 \tag{46}$$

where $\dot{V}_{EX,MX}$ for shallow circular vents is obtained from Epstein [2]

$$\dot{V}_{EX,MX} = 0.055(4/\pi)A_V(gD|\varepsilon|)^{1/2} \tag{47}$$

and where the yet-undetermined values for m_2 and m_1 are

$$m_2(\varepsilon) = d(\dot{V}_L^{(1)}/\dot{V}_{EX,MX})/d(\Delta p/\Delta p_{FL}^{(1)})|_{\Delta p/\Delta p_{FL}^{(1)} = 0}$$
$$m_1(\varepsilon) = m_2(\varepsilon)\dot{V}_{EX,MX}/\dot{V}_{H,FL}^{(1)} \tag{48}$$

Following the above, $\dot{V}_H^{(1)}/\dot{V}_{H,FL}^{(1)}$, $\dot{V}_L^{(1)}/\dot{V}_{H,FL}^{(1)}$, and $\dot{V}_N^{(1)}/\dot{V}_{H,FL}^{(1)}$ vs $\Delta p/\Delta p_{FL}^{(1)} \leq 1$ are sketched in Figure 9.

Presented in Table 3 are flow rate data from Epstein and Kenton [4] for circular vents or disks (L/D = 0.0190 and 0.113) and tubes (0.39 ≤ L/D ≤ 5.0) in a limited portion of the mixed flow regime. The reported data have "experimental uncertainty ... between 10 and 30 percent." Difficulty in acquiring accurate data relatively close to the uni-directional flow regime ($\dot{V}_N^{(1)}/\dot{V}_{H,FL}^{(1)} > 0.6$, $0 \leq \dot{V}_L^{(1)}/\dot{V}_{EX,MX} < 0.1$) apparently precluded measurements of flow in this range.

Since the ε-range of Table-3 is so narrow ($0.12 \leq \varepsilon \leq 0.16$), the data cannot be used to determine ε-dependence of m_2 that may exist. Accordingly, m_2 is approximated as a constant.

Using Eqs. (43') in (44') leads to $\dot{V}_L^{(1)}/\dot{V}_{EX,MX}$ as a function of $\dot{V}_N^{(1)}/\dot{V}_{H,FL}^{(1)}$. The m_2 value providing a least-squares fit of this function to small-L/D data pairs of Table 3 is found to be

$$m_2 = - 0.7070 \text{ (best fit for L/D = 0.0190 and 0.112}$$
$$\text{data of Epstein and Kenton [4]) } \tag{49}$$

Eqs. (43)-(49) are the model equations for the mixed flow regime.

Vent Type	D	L/D	$\dot{V}_N^{(1)}/\dot{V}_{H,FL}^{(1)}$ {1}	$\dot{V}_L^{(1)}/\dot{V}_{EX,MX}$ {1}
disk	0.02540	0.01902	0.5331	0.1743
disk	0.02540	0.01902	0.4329	0.2729
disk	0.02540	0.01902	0.1068	0.7588
disk	0.02540	0.1130	0.2996	0.5270
tube	0.02540	0.5000	0.09279	0.6917
tube	0.02540	0.5000	0.2936	0.3108
tube	0.02540	1.000	0.1957	0.5045
tube	0.02540	1.000	0.5661	0.1180
tube	0.02540	1.000	0.4541	0.1504
tube	0.02540	1.000	0.2113	0.4741
tube	0.02540	2.000	0.4659	0.1728
tube	0.02540	2.000	0.5088	0.1362
tube	0.02540	2.000	0.2663	0.2920
tube	0.02540	5.000	0.1992	0.5693
tube	0.02540	5.000	0.4456	0.2213
tube	0.02540	5.000	0.2442	0.4428
tube	0.04450	0.3910	0.0998	0.7067
tube	0.04450	0.3910	0.4983	0.1472
tube	0.04450	0.3910	0.3049	0.3706
tube	0.04450	0.3910	0.2190	0.4821

{1} $\dot{V}_N^{(1)}$ and $\dot{V}_L^{(1)}$ are from Table 2 of Epstein and Kenton [4]; $\dot{V}_{EX,MX}$ and $\dot{V}_{H,FL}^{(1)}$ are from Eqs. (20) and (21) of Epstein and Kenton [4], respectively.

TABLE 3. $\dot{V}_N^{(1)}/\dot{V}_{H,FL}^{(1)}$ vs $\dot{V}_L^{(1)}/\dot{V}_{EX,MX}$ RESULTS ·FROM EPSTEIN AND KENTON [4] IN MIXED FLOW REGIME FOR CIRCULAR VENTS OR DISKS AND TUBES.
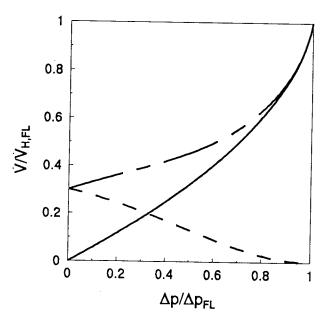

FIGURE 9. SKETCH OF $\dot{V}_H^{(1)}/\dot{V}_{H,FL}^{(1)}$ - - - -; $\dot{V}_L^{(1)}/\dot{V}_{H,FL}^{(1)}$, - -, and $\dot{V}_N^{(1)}/\dot{V}_{H,FL}^{(1)}$ ——, AS FUNCTIONS OF $\Delta p/\Delta p_{FL}$ IN THE MIXED FLOW REGIME.

Additional Comments Regarding Mixed Flow Data

$\dot{V}_L^{(1)}/\dot{V}_{EX,MX}$ vs $\dot{V}_N^{(1)}/\dot{V}_{H,FL}^{(1)}$ from Eqs. (43'), (44'), (46), and (49) is plotted in Figure 10. Also included are all data of Table 3. It is interesting to note that these data, the bulk of which involve flow through tube-like vents (i.e., moderate-to-large L/D) rather than shallow vents, are well correlated by the m_2 of Eq. (49), established from the few, available, shallow-vent data.

The m_2 value providing the least-squares fit of *all* data of Table 3 has also been determined

$m_2 = -1.8077$ (best fit for all data of Epstein and Kenton [4], $0.0190 \leq L/D \leq 5.0$) (49')

and $\dot{V}_L^{(1)}/\dot{V}_{EX,MX}$ vs $\dot{V}_N^{(1)}/\dot{V}_{H,FL}^{(1)}$ from Eqs. (43'), (44'), (46), and (49') is also plotted in Figure 10.

It is of interest to define

$m_3 = d(\dot{V}_L^{(1)}/\dot{V}_{EX,MX})/d(\dot{V}_N^{(1)}/\dot{V}_{H,FL}^{(1)})|_{\dot{V}_N^{(1)}/\dot{V}_{H,FL}^{(1)} = 0}$

$= [2m_2 M/(M + 1)]$

$= -1.2781$ [m_2 from Eq. (49)];   (50)

$= -2.625$ [m_2 from Eq. (49')]

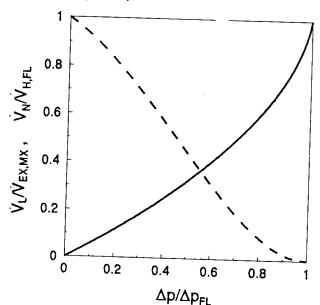These can be compared to $m_3 = -2.5$ of Eq. (22), of Epstein and Kenton [4], namely,[2]

FIGURE 10. PLOTS OF $\dot{V}_L^{(1)}/\dot{V}_{EX,MX}$ AND $\dot{V}_N^{(1)}/\dot{V}_{H,FL}^{(1)}$ AS FUNCTIONS OF $\Delta p/\Delta p_{FLOOD}^{(1)}$ ACCORDING TO EQS. (51), (53'), (54), AND (57).

[2]The 2.5 exponent in Eq. (51) is different than that of Eq. (23) of Epstein and Kenton [4] which seems to be printed incorrectly. Eq. (51) corresponds to the correlating function plotted in Figure 5 of [4].

$$\dot{V}_L^{(1)}/\dot{V}_{EX,MX} = (1 - \dot{V}_N^{(1)}/\dot{V}_{H,FL}^{(1)})^{2.5} \qquad (51)$$

A plot Eq. (51) is included in Figure 11.

VENTCL2 - AN ALGORITHM FOR COMBINED BUOYANCY- AND PRESSURE-DRIVEN FLOW THROUGH HORIZONTAL VENTS

For unstable cross-vent densities, the above leads to the following algorithm, called VENTCL2, for calculating $\dot{V}_N$, $\dot{V}_L$, and $\dot{V}_H$ through small-L/D circular vents:

1. Verify that $\rho_T > \rho_B$, i.e., the configuration is unstable, and calculate $\Delta\rho$ from Eq. (3); determine $\bar{T}$ from Eq. (10) and $\mu(\bar{T})$ from note {6} of Table 1; determine $\varepsilon > 0$ and $\bar{\rho}$ from Eq. (15).

2. Determine p_H and p_L, Δp, and $\bar{p}$ from Eqs. (1) and (2); according to Figure 1 designate the problem type as either Problem 1 or 2, involving Configuration 1 or 2, respectively; if it is Configuration 2, then replace ε by $-\varepsilon < 0$.

3. Determine $\overline{Gr}$ from Eq. (15) and verify that $\overline{Gr}$ satisfies the large-$\overline{Gr}$ criterion, $\overline{Gr} \geq 2(10^7)$.

4. Calculate $\overline{Fr}_{H,FL}^{(1)}$ and then $\dot{V}_{H,FL}^{(1)}$ from Eqs. (31) and (41), $\Delta p_{FL}^{(1)}$ from Eq. (32'), and $\Delta p/\Delta p_{FL}^{(1)}$.

5. If $\Delta p/\Delta p_{FL}^{(1)} \geq 1$, expect uni-directional flow. Estimate $\dot{V}_L = \dot{V}_L^{(1)} = 0$ and $\dot{V}_H = \dot{V}_H^{(1)}$ from Eq. (39) and (40).

6. If $\Delta p/\Delta p_{FL} < 1$, expect mixed flow. Estimate: $\dot{V}_N = \dot{V}_N^{(1)}$ from Eqs. (43) and (46); $\dot{V}_{EX,MX}$ and then $\dot{V}_L = \dot{V}_L^{(1)}$ from Eqs. (45), (44'), and (49); and $\dot{V}_H = \dot{V}_H^{(1)}$ from Eq. (50).
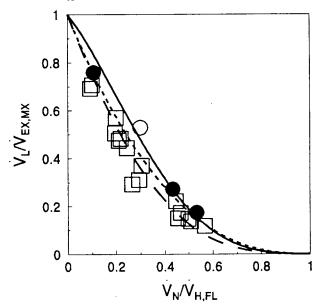

FIGURE 11. PLOT OF $\dot{V}_L^{(1)}/\dot{V}_{EX,MX}$ AS A FUNCTION OF $\dot{V}_N^{(1)}/\dot{V}_{H,FL}^{(1)}$ FROM EQS. (52'), (53'), (54), AND (57), ——; EQS. (52'), (53'), (54), AND (57'), – – –; AND EQ. (60), ·····. PLOT OF DATA OF EPSTEIN AND KENTON [4], I.E., TABLE 3 (L/D = 0.0190 VENT, ●; L/D = 0.113 VENT, ○; AND TUBES WITH 0.39 ≤ L/D ≤ 5.0, □)

The algorithm is suitable for horizontal vent flow calculations, in general, and for use in zone-type compartment fire models, in particular.

NOMENCLATURE

A_V	vent area
C_D; $C_D^{(N)}$;	vent flow coefficient, Eq. (4); C_D for Problem N; C_D of [6]; C_D at large Re number;
$C_{D,HS}$; $C_{D,\infty}$;	C_D at onset of flooding
$C_{D,FL}$	
C_p	specific heat at constant pressure
D	characteristic span of vent opening, diameter
Fr_{HS}	Eq. (9), Froude number of [7]
$Fr_H^{(N)}$, $\overline{Fr}_L^{(N)}$;	Froude numbers for Problem N, Eqs. (20) and (21); $\overline{Fr}_H^{(N)}$ at onset of flooding
$\overline{Fr}_{H,FL}^{(N)}$	
Gr_{HS}; $\overline{Gr}$	Eq. (9), Grashof number of [7]; Grashof number, Eq. (15)
g	acceleration of gravity
k	thermal conductivity
L	depth of vent
M	Eqs. (43) and (46)
m_N	Eqs. (46) and (48) for N = 1; Eqs. (44') and (48) for N = 2; Eq. (50) for N = 3
p; $p^{(N)}$; $p^{*'(N)}$;	pressure; p for Problem N; dimensionless $p^{(N)}$, Eq. (14); far-field p on high-, low-pressure p_H, p_L side of vent, near the vent elevation
$\bar{p}$	$(p_H + p_L)/2$
Pr	Prandtl number, Eq. (16)
R	gas constant
T; $T^{(N)}$; $T^{*'(N)}$;	absolute temperature; T for problem N;
T_T, T_B	dimensionless $T^{(N)}$, Eq. (14); far field T in top, bottom space
$\bar{T}$	$(T_T + T_B)/2$
$U_i^{(N)}$; $U_i^{*(N)}$;	velocity for Problem N; dimensionless $U_i^{(N)}$,
$\bar{U}_3^{(N)}$	Eq. (14); average $U_3^{(N)}$ at vent, Eq. (19)
$\dot{V}_{EX}$; $\dot{V}_{EX,MX}$	exchange flow rate, $\dot{V}_L$; maximum $\dot{V}_{EX}$, i.e., at $\Delta p = 0$
$\dot{V}_H$; $\dot{V}_{FL}$;	volumetric flow rate from high- to low-pressure side of vent; $\dot{V}_H$ at onset of flooding;
$\dot{V}_{H,ST}$	$\dot{V}_H$ for standard flow model
$\dot{V}_L$; $\dot{V}_{L,ST}$	volumetric flow rate from low- to high-pressure side of vent; $\dot{V}_L$ for standard flow model
$\dot{V}_H^{(N)}$; $\dot{V}_{H,FL}^{(N)}$	$\dot{V}_H$ for Problem N, Eq. (19); $\dot{V}_H^{(N)}$ at onset of flooding
$\dot{V}_N$; $\dot{V}_N^{(N)}$	$\dot{V}_H - \dot{V}_L$; $\dot{V}_N$ for Problem N
$X_i^{(N)}$; $X_i^{*(N)}$	cartesian coordinates for Problem N, Figure 2; dimensionless $X_i^{(N)}$, Eq. (14)

$\Delta p, \Delta p_{FL}$; $\Delta p_F^{(N)}$	p_H - p_L; Δp at onset of flooding; Δp_{FL} for Problem N
ΔT	T_B - T_T
$\Delta \rho$	ρ_T - ρ_B
ε	dimensionless $\Delta \rho$, ΔT, Eq. (15)
μ; $\bar{\mu}$	dynamic viscosity; Eq. (10)
ν	kinematic viscosity, Table 1
Π; $\Pi_F^{(N)}$	dimensionless Δp, Eq. (16); dimensionless $\Delta p_F^{(N)}$, Eq. (25)
ρ; $\rho^{(N)}$; $\rho^{*'(N)}$; ρ_T, ρ_B	density; ρ for Problem N; dimensionless $\rho^{(N)}$, Eq. (14); far-field ρ in top, bottom space
$\bar{\rho}$	$(\rho_T + \rho_B)/2$
$\sigma_H^{(N)}, \sigma_L^{(N)}$	Eq. (18)
σ_1, σ_2	Eqs. (38) and (39)

REFERENCES

1 Taylor, G. I., The Instability of Liquid Surfaces When Accelerated in a Direction Perpendicular to Their Planes, Proc. Roy. Soc., A, 201, pp. 192-196, 1950.

2 Epstein, M., Buoyancy-Driven Exchange Flow Through Small Openings in Horizontal Partitions, J. Heat Transfer, 110, pp. 885-893, 1988.

3 Brown, W.G., Natural Convection Through Rectangular Openings in Partitions - 2. Horizontal Partitions, Int. J. Heat Mass Transfer, 5, pp. 869-878, 1962.

4 Epstein, M. and Kenton, M.A., Combined Natural Convection and Forced Flow Through Small Openings in a Horizontal Partition With Special Reference to Flows in Multicomparment Enclosures, J. Heat Transfer, 111, pp. 980-987, 1989.

5 Tan, Q. and Jaluria, J., Flow Through Horizontal Vents as Related to Compartment Fire Environments, Rutgers University Report to NIST, National Institute of Technology, Gaithersburg MD, December 1991.

6 Perry, J.A., Critical Flow Through Sharp-Edged Orifices, Trans. American Soc. Mech. Eng., 71, pp. 757-764, 1949.

7 Heskestad, G. and Spaulding, R.D., Inflow of Air Required at Wall and Ceiling Apertures to Prevent Escape of Fire Smoke, Proceedings of the 3rd International Symposium on Fire Safety Science, Elsevier, pp. 919-928, 1991.

8 Cooper, L.Y., Combined Buoyancy- and Pressure-Driven Flow Through a Horizontal Vent: Theoretical Considerations, NISTIR 5252, National Institute of Technology, Gaithersburg MD, 1993.

9 Hilsenrath, J., et al, Tables of Thermal Properties of Gases, NBS circular 564, National Institute of Standards and Technology (presently the National Institute of Standards and Technology), Gaithersburg MD, Nov. 1955.